2014 IEEE/RSJ International Conference on
Intelligent Robots and Systems (IROS 2014)
September 14-18, 2014, Chicago, IL, USA

A new coefficient-adaptive orthonormal basis function model structure for identifying a class of pneumatic soft actuators

Xiaochen Wang[1,*], Tao Geng[1], Yahya Elsayed[1], Tommmaso Ranzani[2], Chakravarthini Saaj[1], Constantina Lekakou[1]

***Abstract*—The class of Pneumatically-driven Lower-pressure Soft Actuators (PLSA) is a popular research topic as it can be potentially used in the surgical robotic applications. One fundamental problem lying in the PLSA research is the lack of a generally validated model for the complex nonlinear dynamic behaviours. In this paper, a new coefficient-adaptive orthonormal basis function model structure is specifically developed for the identification of the general PLSAs. It is a parameter-independent way directly used to identify the dynamic relation between the actuating pressures and the principal degrees of freedom of a PLSA, the bending and the steering. The approach is based on a modified auxiliary kinematic setting. Following the discussion of the identification procedure, the implementations for the double chamber bending and steering are demonstrated. The results show that the proposed approach can accurately capture the nonlinear pressure-shape dynamics. The approach is also efficient in the real-time applications. It can be further used to improve the current control design for the PLSAs in robotic applications.**

I. Introduction

In the fields of surgery and therapy, soft robotic instruments have increasingly attracted the attention of researchers in the past 20 years. Compared with traditional rigid ones, the soft robots can potentially give a more viable solution when the operation is taken in human bodies. The inherent compliance offers human friendly interaction; the kinematic redundancy provides the manoeuvre competency in highly unstructured in-body organ environments. Figure 1 shows three typical PLSA examples. The PLSA is distinguished from the Pneumatic Muscle Actuators (PMA) in a compact design and a lower operating pressure, i.e. less than 2 bar. But they are both in the class of the pneumatically-driven soft continuum robots, and share many similar properties.

For the general pneumatic soft continuum robots, the kinematic modelling is still the backbone in the state-of-the-art control designs [1], [2], [3], [4], [5]. Completely validated dynamic modelling for a single section of the pneumatic soft robot arms is lagging behind. The potential applicability is therefore restricted. The modelling has been analytically

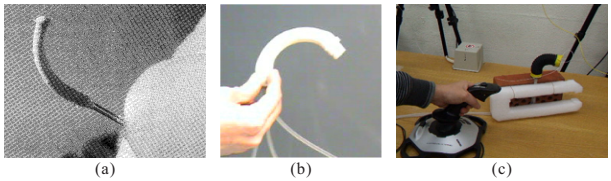

(a) (b) (c)

Fig. 1. Featured PLSA prototypes: (a) Flexible Micro-Actuator by [9]. (b) Colobot by [3]. (c) An early design of the STIFF-FLOP actuator.

studied in [6], [7]. The Lagrange formation under the constant curvature condition was used to derive the dynamic relation between the individual chamber lengths and the shape. The worked models are ineffective in handling the coupling effect between each chamber. Unlike the PMAs, this internal effect can not be neglected in the PLSA cases, because the latter are structured in one integral rubber material. The radial expansion of each individual chamber is not constrained like the way that the individual bellow suits are used in a PMA. Besides, the above modellings do not include the complex nonlinear dynamic relation between the actuating pressures and the chamber lengths, which is an independent open problem too. A recent work by [8] started to tackle the issue of lacking the actuator dynamics based on the previous work in [7]. The proposed model correctly accounts for the identified hysteretic behaviour using the Bouc-Wen restoring force method. This research is on the right track, but it is mainly investigated for the PMAs. Due to the structural difference, the involved intermediate step of the separate pressure-elongation identification for a PMA's individual bladders can not be applied to the internal chambers of a PLSA. And the internal coupling issue has not been formally studied. Besides, another work by [9] directly used a second-order linear transfer function to approximate the pressures-shape relation. But only the single chamber bending situation was partially studied. The model is only valid for a small degree of bending. The deformation was measured based on the deflection distance projected onto the horizontal base plane. However this kinematic variable does not naturally represent the bending deformation in a linear manner.

This paper proposes a unified identification approach for the general PLSAs. For a single section PLSA, it can practically give accurate modelling for the nonlinear dynamics between the actuating pressures and the two principal Degrees Of Freedom (DOF), the bending and the steering. This statistic identification approach is based on a new developed

*E-mail: xiaochen.wang@me.com
[1]Address: Faculty of Engineering and Physical Sciences, University of Surrey, Guildford, GU2 7XH, United Kingdom
[2]Address: The BioRobotics Institute, Sant'Anna School of Advanced Studies, Piazza Martiri della Libert, 33, Pisa, Italy

This work described in this paper is partially funded by STIFF-FLOP project grant from the European Commission Seventh Framework Programme under agreement 287728.

978-1-4799-6934-0/14/$31.00 ©2014 IEEE

coefficient-adaptive orthonormal basis function (OBF) model structure. And a modification is taken in the kinematic setting, which results in a more feasible implementation for the current gyroscopic sensor technology. The proposed approach does not require any specific mechanical parameters such as the elasticity or the chamber dimensions. The resultant model can be further used for incorporation within the following work on the PLSAs such as the control design and the external disturbance analysis.

II. The PLSAs

A. The structure of a single segment PLSA

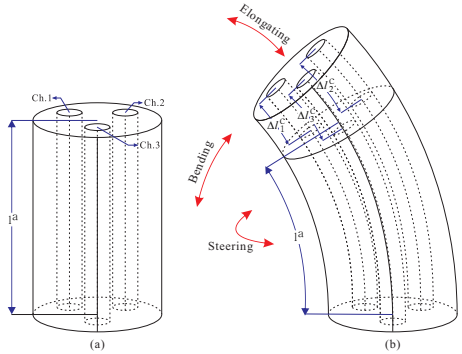

Fig. 2. (a) A simplified structural drawing for the PLSAs at inactive state. (b) The illustration of the bending forced by actuation. In both cases, the braid wearing is omitted.

This paper will focus on the general 3-chamber PLSA design [10] as sketched in Figure 2-(a). Optimally, it is to be designed in a very symmetric way. Three identical pneumatic chambers are regularly disposed at 120° apart, and they are together parallel to the central longitudinal axis of the actuator. Figure 2-(b) gives a brief explanation for the ideal bending. The outer covering of a PLSA usually wears a kind of bellow suits so that the radial expansion induced by the fed-in pressure is largely reduced and can be neglected. The individual chamber elongations are the main type of the deformations structured by the bellow. Thereby they deterministically drive the deformation of the entire actuator. The related DOFs are classified as *bending*, *steering*, and *elongating*.

B. The observed nonlinearities

Figure 3 shows a typical example of the single chamber deflection/bending-actuation relation from our experiments. The test consists of 28 local step responses, each of which starts the initial condition from its predecessor's final condition. And both the pressure increase and the decrease situations are taken. The state-of-the-art nonlinear identification model structures might appear to be deficient to describe the combined static and dynamic observed below. This leads us to develop a new model structure of identification.

The first type of nonlinearity that can be spotted is the dead-zone effect at the initial pressure range. It is due to the gas fill-in phase during the initial actuation. Secondly, in the pressure

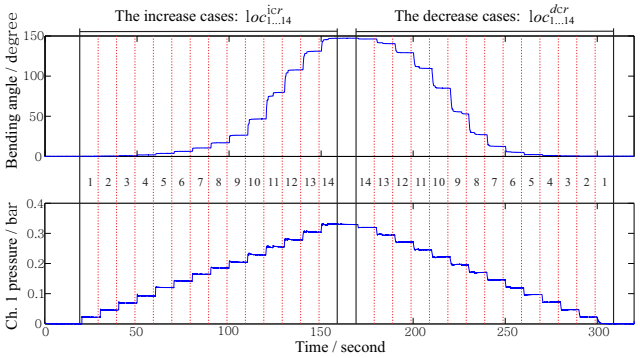

Fig. 3. Globally conducted local step responses.

increase cases, it can be seen that the steady state values of each local step response are not in a linear relations with their input ones. The similar situations happen in the pressure decrease cases. By further comparing both the increase and the decrease cases, it is not hard to figure out an underlying hysteresis loop. The cause of the static nonlinearity roots in the nonlinear elongation-pressure relation of a chamber or bladder. Especially the hysteresis effect is due to the friction with the braid [11], [12], [13]. At last, we extracted the data sets of the increase cases, removed their offsets on both the input and output channels, and then put them together aligned to a same trigger time. The post-analysis showed that all those data sets can be very well linearised, but each linearised model is formed in an inconsistent model structure with others and they behave in different transient responses. They have very similar increments at the input channel. However as indicated from the output channel, the slopes under the local responses became increasingly steep as the operating pressure rose step by step. A similar result was also obtained in the decrease cases. In run time, varying the fed-in pressure alters the actuator's stiffness, which is the main reason that causes the dynamic nonlinearity here. On the other hand, the analysed static and the dynamic nonlinearities also inherit in the cases when operating more than one chambers. Additionally, new types of nonlinearities are introduced due to the coupling effect between the active chambers.

III. Fundamental Theories

In order to capture the nonlinearities discussed in Section II-B, a new model structure will be developed later in Section V-B. Its backbone is OBF and the Fuzzy Kolmogorov c-Max (FKcM) clustering algorithm.

A. The OBFs in the linear system identification

A stable and strictly proper transfer function $G(q)$ can be decomposed into a series expansion of OBFs $\{\mathcal{B}_i(q)\}_{i=1}^{\infty}$ with coefficient $\{c_i\}_{i=1}^{\infty}$. By an appropriate truncation on the series of $\{\mathcal{B}_i(z)\}_{i=1}^{\infty}$, the approximation for the general linearisable systems in the input/output form can be expressed as

$$y_k \approx \sum_{i=1}^{n} c_i \mathcal{B}_i(q) u_k \tag{1}$$

where u_k and y_k are a pair of observed input and output. The construction for a set of OBFs relies on the general repetitive pole structure $\{\xi_1, ..., \xi_{n_b}, \xi_{n_b+1}, ..., \xi_{n_b+n_b}, ..., \}$. According to it, the individual OBFs can be constructed in a unified and iterative approach [14] as

$$\mathcal{B}_i(q) = \frac{\sqrt{1-|\xi_i|^2}}{q-\xi_i} \prod_{k=0}^{i-1} \frac{1-\overline{\xi_k}q}{q-\xi_k}, \tag{2}$$

where embedded inner function of (2) is

$$G_b(q) = \prod_{j=1}^{n_b} \frac{1-\overline{\xi_k}q}{q-\xi_k}. \tag{3}$$

The convergence rate of the series expansion is bounded by the decay rate $\rho = \max_k |G_b(\xi_k^{-1})|$. A smaller decay rate will imply a less approximation error. The selected poles become optimal when they get close to the actual system poles [14].

B. The FKcM algorithm for the OBF pole selection

It is crucially important to select an appropriate pole set when building up the OBF model structure (1), because the underlying pole set determines the convergence rate of the truncated series expansion. The solution was sought by [15] in the scope of Fuzzy c-Mean clustering, where the pole selection problem is transformed to a fuzzy-functional expression as

$$J_m(U,V) \triangleq \max_{k \in \mathbb{I}_1^{N_z}} \sum_{i=1}^{n_c} \mu_{ik}^m d_{ik}. \tag{4}$$

In the formulation, $V = [v_i]_{i=1}^{n_c}$ is the vector of the cluster centres; $U = [\mu_{ik}]_{n_c \times n_z}$ is the membership matrix; m is the fuzziness which is a design parameter; d_{ik} is the distance to measure the dissimilarity between a v_i and an identified pole z_k. Especially d_{ik} is the 1-width version of (3). (4) is a worse-case criterion, and minimizing it on an identified pole set $Z = \{z_k\}_{k=1}^{N_z}$ leads to the argument of the Kolmogorov n-Width membership matrix and the cluster center vector $(\hat{U}, \hat{V}) = \arg\min J_m$. $\hat{V}$ is to be used for the OBF construction. The FKcM algorithm is studied in [16].

IV. Kinematic Modelling

A. The modified auxiliary setting

As shown in Figure 4, the constant curvature condition is generally held in the PLSAs. The orientation of the tip surface can be equivalently mapped to the DOF of the bending and the steering. We base this and develop a different setting for the configuration space parameter. The new setting can be be implemented by on-shelf gyroscopic sensors which is low-cost and easier than current means like fibre-sensors, visual tracking. The setting is effective in capturing the bending and the steering dynamics. It can serve as an accessory along the mainstream approach in [17].

An overall view of the new auxiliary setting is illustrated in Figure 5. The modification takes place at the robot-dependent mapping part; the part of the robot-independent mapping is kept unchanged. The actuator space is replaced by three *configuration subspaces* as shown in Figure 5. In this setting, the scenario of the actuation by any two certain chambers is uniquely confined to each of the subspaces. The three configuration subspaces are defined on the same polar plane that is for the configuration space; the latter is divided by the former. Each of the three configuration subspaces is a fan-shaped area, and its two radial boundaries are defined where the two chambers' singly-driven deflections project onto the polar plane. Every individual configuration subspace consists of a deflection angle θ_i and a steering angle ϕ_i^{sub} to represent the deflection and the steering. As the equivalence to the tip surface orientation, the term arc length l^a is not used to estimate the bending and the steering. Under the constant curvature condition the deflection angle θ^d is equal to the bending angle θ^b. Figure 6 shows the modified kinematic framework.

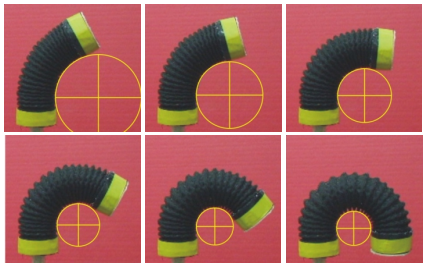

Fig. 4. The demonstration for the constant curvature condition on a PLSA in this study. Under 6 different pressures, the test PLSA is all under a different but constant curvature.

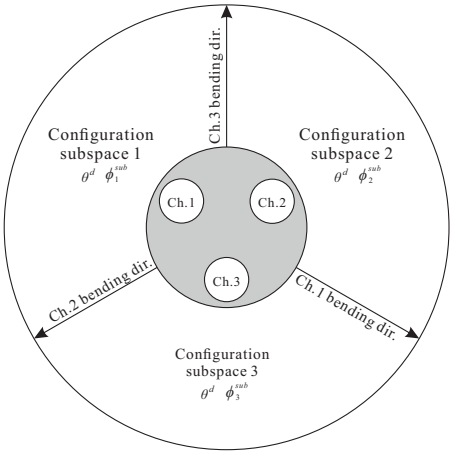

Fig. 5. The illustration for the three configuration subspace 1, 2 and 3. They are sectioned by the three chambers' individual bending directions.

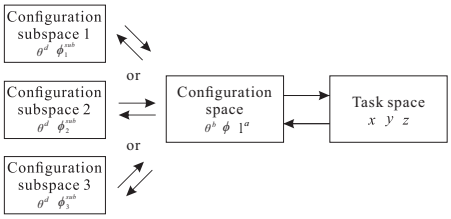

Fig. 6. The modified auxiliary kinematic framework for the PLSA actuators.

On the other hand, the new auxiliary setting can well incorporate with the current elongation measurement to estimate the task space parameters. A PLSA's length can be accurately measured by the optical fibre sensors as in [3], or be estimated by the polynomially pre-identified pressure-length relation. With an acquired tube length l^a and the bending and the steering angles θ^b and ϕ obtained from this proposed auxiliary approach, one can use the summarised constant curvature approach in [17] to easily estimate the task space parameters x, y and z.

B. The calculation for the deflection and the steering angles

Our modified configuration is based on the Trackstar™ magnetic sensor. It has a sensing base and a sensing tip. The base provides the global reference frame G, and it is fixed at a place during operation. The sensing tip is attached with the local reference frame B, and it is installed perpendicular to the tip surface of a PLSA. The setting is illustrated in Figure 7. It can be adopted by the gyroscopic sensors with minor adjustments.

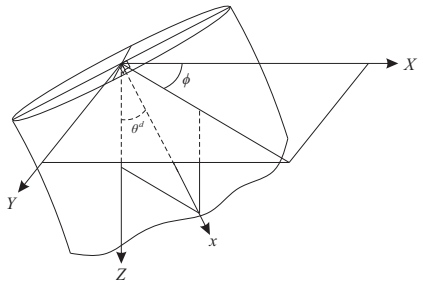

Fig. 7. The reference frame configured at a PLSA's tip end. It is based on the Trackstar™ magnetic sensor.

The degree of the deflection is equivalent to the intersection angle between ${}^B_G e_Z$ and ${}^B e_x$ which can be calculated as

$$\theta^d = \arccos(\langle {}^B e_x, {}^B A_G {}^G e_Z \rangle) \tag{5}$$

where ${}^B e_x = \begin{bmatrix} 1 & 0 & 0 \end{bmatrix}^T$ and ${}^G e_Z = \begin{bmatrix} 0 & 0 & 1 \end{bmatrix}^T$. The local frame yaw-pitch-roll rotation matrix is used according to the sensor-specific triple rotation ${}^B A_G$.

The steering angle is the intersection angle between the projection of ${}^B e_x$ onto the OXY plane and X-axis, or alternatively Y-axis. The calculation is expressed as

$$\phi = \arctan\left(\frac{\langle {}^B e_x,\ {}^B A_G\ {}^G e_Y \rangle}{\langle {}^B e_x,\ {}^B A_G\ {}^G e_X \rangle}\right) \tag{6}$$

where ${}^B e_x = \begin{bmatrix} 1 & 0 & 0 \end{bmatrix}^T$, ${}^G e_X = \begin{bmatrix} 1 & 0 & 0 \end{bmatrix}^T$ and ${}^G e_Y = \begin{bmatrix} 0 & 1 & 0 \end{bmatrix}^T$.

V. The Model Identification Setting

A. The experimental design

The system identification approach is proposed in the bottom-up fashion. The local data sets are identified at first and they will be combined together to reconstruct the global responses. The motivation comes from the fact that each local data set can be fairly linearised. Using them would lead to a globally accurate dynamic description. In the multiple-chamber bending and steering cases, the identification test is arranged in a decoupled way. Each time only one of the input channels is allowed to exert a local step response, meanwhile the responses on the output channels are being sampled. In this way, the Single-Input-Multiple-Output (SIMO) models can be separately identified with respect to each input channel. They will be used to approximate the complete Multiple-Input-Multiple-Output (MIMO) model in a local interval.

B. The DIO-PWL-OBF model structure

In the light of the local approach, a new nonlinear OBF model structure specified for the PLSA identification is going to be developed. It is named as Difference Input Output, PieceWise Linear, Orthonormal Basis Function (DIO-PWL-OBF) model structure as the indication of the three involved theoretical constituents.

The starting point of the development is the Linear Parameter-Varying (LPV) -OBF model structure [16]. The scheduling part is updated based on a floating reference point, whereas our approach uses a number of fixed ones. By bringing it to the PWL sense, the model structure is modified as

$$y_k \approx \sum_{i=1}^{n} c_i^l \mathcal{B}_i(q) u_k,\ l \in N_{Loc}, \tag{7}$$

There are two issues regarding (7). The first issue is the switching effect. It happens during the transition from one local region to another. If the post local model structure hardly follows the previous one in a consistent manner like in a same order or having similar frequency characters, a relatively large modelling error will be caused. The second issue is the offset effect. It is caused by the initial and final conditions in each sampled local data set. In the designed experiment, the system starts and ends at two equilibrium points in each of the partitioned local regions. This will lead to two steady-state simultaneous equations in the linear regression process. As the PLSA system is not globally linear, the coefficient sets of a local model will extend to a relatively long size in solving the related linear equations.

To tackle the two issues, the Difference Input and Output (DIO) time series are defined as

$$\begin{array}{ll} {}_\delta y_k \triangleq y_k - y_{k-1}, & {}_\delta y_1 \triangleq y_1 \\ {}_\delta u_k \triangleq u_k - u_{k-1}, & {}_\delta u_1 \triangleq u_1 \end{array}, \tag{8}$$

based on the input and output time series, $\{u_k\}$ and $\{y_k\}$. $\{\delta u_k\}$ and $\{\delta y_k\}$ represent the immediate change between every two neighbour sampling points in $\{u_k\}$ and $\{y_k\}$. The relation between the former and the latter is

$$u_k = \sum_{n=1}^{k} \delta u_n,\ y_k = \sum_{m=1}^{k} \delta y_m. \tag{9}$$

By substituting (9) into the standard Ordinary Difference Equation (ODE) form (10),

$$\sum_{i=0}^{n_a} a_i q^{-i} y_k = \sum_{j=1}^{n_b} b_j q^{-j} u_k, \tag{10}$$

one can get

$$a_0 \sum_{1}^{k} \delta y_m + \ldots + a_1 \sum_{1}^{k-i} \delta y_m = b_1 \sum_{1}^{k-1} \delta u_n + \ldots + b_j \sum_{1}^{k-j} \delta u_n, \tag{11}$$

which is the ODE in the DIO sense. (11) can be further decomposed into a set of simultaneous equations as

$$\begin{cases} a_0\delta y_k & +\ldots+ a_i\delta y_{k-i} = b_1\delta u_{k-1} + \ldots + b_j\delta u_{k-j} \\ \vdots & \vdots \quad \vdots & \vdots \quad \vdots \\ a_0\delta y_{i+1} + \ldots + a_i\delta y_1 & = b_1\delta u_j & + \ldots + b_j\delta u_1 \\ \vdots & \vdots \quad \vdots & \vdots \quad \vdots \\ a_0\delta y_2 & +\ldots+ \quad 0 & = b_1\delta u_1 \quad +\ldots+ \quad 0 \end{cases}. \tag{12}$$

Compared with the orthodox expression (10), the derived one (12) could give us a different insight into the dynamics of a system. Instead of $\{u_k\}$ and $\{y_k\}$, the input and output channels are now viewed in the definition of $\{\delta u_k\}$ and $\{\delta y_k\}$. The entire dynamics of a system can be interoperated as the composition of all the individual DIO impulse responses by per sampling point forward along the time line. The dynamic responses of each δu_k can be individually evaluated. In the nonlinear systems, this feature is very appreciated because it gives an extra degree of freedom to manipulate the dynamics.

By preserving the latest δu_k and δy_k in the first line and arranging the rest into the transfer-function form, (12) can incorporate into (7) as

$$y_k \approx y_{k-1} + \sum_{i=1}^{n} c_i^l \mathcal{B}_i(q)\delta u_k,\ l \in N_{Loc}, \tag{13}$$

which is the final form of the DIO-PWL-OBF model structure. The switching effect is diminished significantly as only the latest DIO sample of δu and δ_y is used in the dynamics evaluation. The previous $\{u\}_1^{k-1}$ and $\{y\}_1^{k-1}$ do not affect the nonlinear estimation. (13) also solves the offset problem. The identified local model can be directly used without adding the offset, which avoids the global static nonlinearty. And the order of the linearised model is relatively lower. The n-step-ahead predicator based on (13) is formulated as

$$\hat{y}(k+n) = y(k) + \sum_{m=k+1}^{k+n} \sum_{i=1}^{n} c_i^l(m)\mathcal{B}_i(q)\delta u(m). \tag{14}$$

Compared with the Hammersten-Wiener (HW) and the nonlinear Auto-Regression with eXogeneous variables (ARX) approaches, this method would be more advantageous for the PLSA identification, because all the local properties of the dynamics are preserved. The simple linear regression is to be solved locally instead of nonlinear one in the global sense. In run time, the switching is taken when the system moves from one locally linearised region to another. The unified identification procedure is summarised in Table I.

TABLE I
THE UNIFIED IDENTIFICATION PROCEDURE.

Step 1	Setup the platform.
Step 2	Select a number of reference pressures on each chamber.
Step 3	Take the identification experiment.
Step 4	Extract, deoffset and linearise the local data sets.
Step 5	Apply the FKcM pole clustering algorithm for the locally identified poles.
Step 6	Construct the OBF set based on the optimally selected poles.
Step 7	Arrange the constructed OBFs in the DIO-PWL-OBF setting.

VI. IMPLEMENTATION AND RESULTS

A. Platform setup

The platform setup is shown in Figure 8. A desktop using Matlab Real-Time Windows Target™ serves as the central platform to interface the other parts. The system works at a sample rate of 80 Hz, and it is constantly supplied with stable 1 bar compressed air. A test PLSA actuator used in the following identification work is made in the silicon rubber and it is 9 cm in length and 3 cm in diameter. The operating pressure of a single chamber is below 0.4 bar. As the constant curvature condition is held satisfyingly, the deflection angle is accurately approximated to the bending angle. The elongation measurement is neglected.

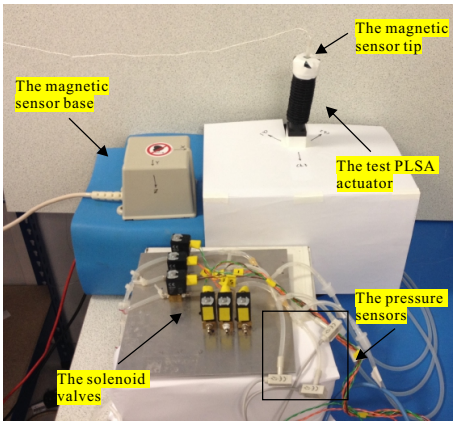

Fig. 8. A photo of the platform

B. Double chamber identification

The identification is conducted by following the instructions in Table I. Chamber 1 and Chamber 2 of the test PLSA are used. As illustrated in Figure 9, the local data sets are partitioned based on different pressure levels of both the chambers. The pressure range for each chamber is set between 0.20 bar and 0.35 bar.

TABLE II
THE POLE SET $\{\xi_1^{ij}, \ldots, \xi_5^{ij}\}_{i=1,2,j=1,2}$ FOR THE OBFS.

Decoupled IO pair (u_i, y_j)	Pole structure $\{\xi_1^{i,j}, \ldots, \xi_5^{i,j}\}$
$u_1 \rightarrow y_1$	0.981, 0.969, 0.964, 0.957, 0.945
$u_2 \rightarrow y_1$	0.986, 0.975, 0.960, 0.950, 0.942
$u_1 \rightarrow y_2$	0.998, 0.979, 0.949, 0.935, 0.884
$u_2 \rightarrow y_2$	0.983, 0.973, 0.961, 0.946, 0.939

After removing the offsets on both the input and output channels in the local data sets, linear analysis is taken individually. The 1-pole-0-zero structure can be properly used for every decoupled SISO dynamic relation. The FKcM clustering is taken for the identified poles of each decoupled SISO pair. The calculated poles are listed in Table II. They are used for the OBF construction.

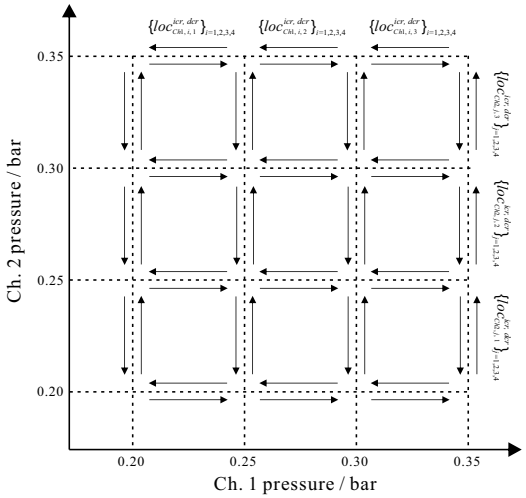

Fig. 9. The local partition for the double chamber identification. The arrows denote the pressure changing direction in each local identification part.

A joystick-based pressure control was applied to the platform, by which, both of the chambers can be actuated. Its validation result is plotted in Figure 10. On average, the Normalized Root-Mean-Square Error (NRMSE) fit results are above 80%. The system's dynamic responses are tracked within tolerable errors. It can be seen the proposed identification approach is applicable in the double chamber cases.

VII. CONCLUSION AND PERSPECTIVES

In this paper, a unified identification approach for the general PLSAs has been presented, and its implementations for the double chamber bending and steering is demonstrated. In the next stage, our research is going to focus on using the acquired identification model to facilitate the control design.

REFERENCES

[1] B. Jones and I. Walker, "Practical kinematics for real-time implementation of continuum robots," *Robotics, IEEE Transactions on*, vol. 22, no. 6, pp. 1087–1099, 2006.

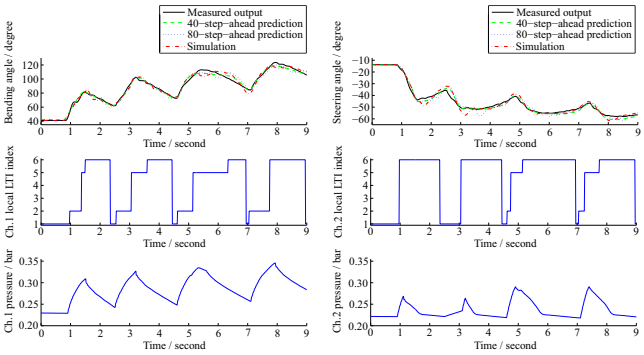

Fig. 10. The joystick-controlled test and validation.

[2] D. Braganza, D. Dawson, I. Walker, and N. Nath, "A neural network controller for continuum robots," *Robotics, IEEE Transactions on*, vol. 23, no. 6, pp. 1270–1277, 2007.

[3] G. Chen, M. Pham, and T. Redarce, "Sensor-based guidance control of a continuum robot for a semi-autonomous colonoscopy," *Robotics and Autonomous Systems*, vol. 57, no. 67, pp. 712–722, 2009.

[4] Y. Bailly, Y. Amirat, and G. Fried, "Modeling and control of a continuum style microrobot for endovascular surgery," *Robotics, IEEE Transactions on*, vol. 27, no. 5, pp. 1024–1030, 2011.

[5] M. Rolf and J. Steil, "Constant curvature continuum kinematics as fast approximate model for the bionic handling assistant," in *Intelligent Robots and Systems, 2012 IEEE/RSJ International Conference on*, 2012, pp. 3440–3446.

[6] E. Tatlicioglu, I. Walker, and D. Dawson, "New dynamic models for planar extensible continuum robot manipulators," in *Intelligent Robots and Systems, 2007. IROS 2007. IEEE/RSJ International Conference on*, 2007, pp. 1485–1490.

[7] I. Godage, D. Branson, E. Guglielmino, G. Medrano Cerda, and D. Caldwell, "Shape function-based kinematics and dynamics for variable length continuum robotic arms," in *Robotics and Automation, 2011 IEEE International Conference on*, 2011, pp. 452–457.

[8] I. Godage, D. Branson, E. Guglielmino, and D. Caldwell, "Pneumatic muscle actuated continuum arms: Modelling and experimental assessment," in *Robotics and Automation, 2012 IEEE International Conference on*, 2012, pp. 4980–4985.

[9] K. Suzumori, S. Iikura, and H. Tanaka, "Flexible microactuator for miniature robots," in *Micro Electro Mechanical Systems, 1991, MEMS '91, Proceedings. An Investigation of Micro Structures, Sensors, Actuators, Machines and Robots. IEEE*, 1991, pp. 204–209.

[10] M. Cianchetti, T. Ranzani, G. Gerboni, I. De Falco, C. Laschi, and A. Menciassi, "Stiff-flop surgical manipulator: Mechanical design and experimental characterization of the single module," in *Intelligent Robots and Systems (IROS), 2013 IEEE/RSJ International Conference on*, Nov 2013, pp. 3576–3581.

[11] C. Chou and B. Hannaford, "Measurement and modeling of mckibben pneumatic artificial muscles," *Robotics and Automation, IEEE Transactions on*, vol. 12, no. 1, pp. 90–102, 1996.

[12] B. Tondu and P. Lopez, "Modeling and control of mckibben artificial muscle robot actuators," *Control Systems, IEEE*, vol. 20, no. 2, pp. 15–38, 2000.

[13] P. Dario, B. Hannaford, and A. Menciassi, "Smart surgical tools and augmenting devices," *Robotics and Automation, IEEE Transactions on*, vol. 19, no. 5, pp. 782–792, 2003.

[14] B. Ninness and F. Gustafsson, "A unifying construction of orthonormal bases for system identification," *Automatic Control, IEEE Transactions on*, vol. 42, no. 4, pp. 515–521, 1997.

[15] R. Tóth, P. Heuberger, and P. V. D. Hof, "Asymptotically optimal orthonormal basis functions for lpv system identification," *Automatica*, vol. 45, no. 6, pp. 1359–1370, 2009.

[16] R. Tóth, *Modeling and Identification of Linear Parameter-Varying Systems - an orthonormal basis function approach*. Springer, 2010.

[17] R. Webster and B. Jones, "Design and kinematic modeling of constant curvature continuum robots: A review," *The International Journal of Robotics Research*, vol. 29, no. 13, pp. 1661–1681, 2010.